Ultrafast Excited State Dynamics in Molecular Motors

Conyard, Jamie; Stacko, Peter; Chen, Jiawen; McDonagh, Sophie; Hall, Christopher R.; Laptenok, Sergey P.; Browne, Wesley R.; Feringa, Ben L.; Meech, Stephen R.

Published in:
The Journal of Physical Chemistry. A: Molecules, Spectroscopy, Kinetics, Environment, & General Theory

DOI:
10.1021/acs.jpca.7b00087

Publication date:
2017

THE JOURNAL OF PHYSICAL CHEMISTRY A

Article

pubs.acs.org/JPCA

Ultrafast Excited State Dynamics in Molecular Motors: Coupling of Motor Length to Medium Viscosity

Jamie Conyard,[†] Peter Stacko,[‡] Jiawen Chen,[‡] Sophie McDonagh,[†] Christopher R. Hall,[†] Sergey P. Laptenok,[†] Wesley R. Browne,[‡] Ben L. Feringa,*[,‡] and Stephen R. Meech*[,†]

[†]School of Chemistry, University of East Anglia, Norwich Research Park, Norwich NR4 7TJ, U.K.

[‡]Stratingh Institute for Chemistry, University of Groningen, Nijenborgh 4, 9747AG Groningen, The Netherlands

Supporting Information

ABSTRACT: Photochemically driven molecular motors convert the energy of incident radiation to intramolecular rotational motion. The motor molecules considered here execute four step unidirectional rotational motion. This comprises a pair of successive light induced isomerizations to a metastable state followed by thermal helix inversions. The internal rotation of a large molecular unit required in these steps is expected to be sensitive to both the viscosity of the medium and the volume of the rotating unit. In this work, we describe a study of motor motion in both ground and excited states as a function of the size of the rotating units. The excited state decay is ultrafast, highly non-single exponential, and is best described by a sum of three exponential relaxation components. The average excited state decay time observed for a series of motors with substituents of increasing volume was determined. While substitution does affect the lifetime, the size of the substituent has only a minor effect. The solvent polarity dependence is also slight, but there is a significant solvent viscosity effect. Increasing the viscosity has no effect on the fastest of the three decay components, but it does lengthen the two slower decay times, consistent with them being associated with motion along an intramolecular coordinate displacing a large solvent volume. However, these slower relaxation times are again not a function of the size of the substituent. We conclude that excited state decay arises from motion along a coordinate which does not necessarily require complete rotation of the substituents through the solvent, but is instead more localized in the core structure of the motor. The decay of the metastable state to the ground state through a helix inversion occurs 14 orders of magnitude more slowly than the excited state decay, and was measured as a function of substituent size, solvent viscosity and temperature. In this case neither substituent size nor solvent viscosity influences the rate, which is entirely determined by the activation barrier. This result is different to similar studies of an earlier generation of molecular motors, which suggests different microscopic mechanisms are in operation in the different generations. Finally, the rate of photochemical isomerization was studied for the series of motors, and those with the largest volume substituents showed the highest photochemical cross section.

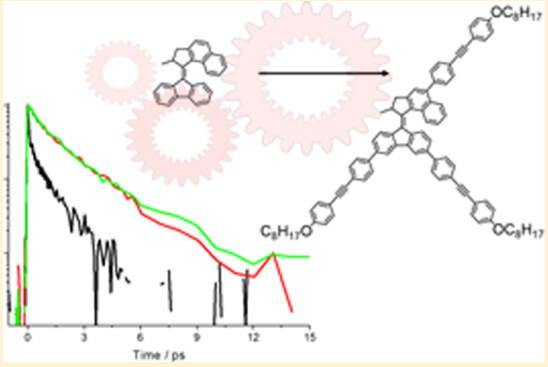

INTRODUCTION

Molecular motors are found throughout nature, playing key roles in a number of essential biological processes.[1] Such biological motors are complex and elegant machines, converting chemical energy to fuel molecular motion with high efficiency. Their discovery inspired a drive in synthetic chemistry and nanotechnology toward the design of molecular systems which afford controllable motion on a molecular scale.[2] In recent years, a number of successful synthetic rotors,[3] motors[4,5] and shuttles[6−10] have been reported using a range of power sources including light, heat and redox chemistry.

One of the most promising designs is the light-driven unidirectional rotary motor based on chiral overcrowded alkenes, pioneered by Feringa and co-workers[11] (**1a** in Figure 1). The motor structure comprises a lower "stator" fluorene ring separated from an upper "rotor" by an olefinic "axle". The fundamental principle which underpins the classification of this system as a true molecular rotary motor (rather than a simple forward/reverse molecular switch) is the fully unidirectional rotation of the rotor relative to the stator. In the overcrowded alkene design, this unidirectionality is achieved via the repetitive two step mechanism shown in Figure 1. First, the initial structure (**1a**) undergoes an excited state isomerization reaction to generate a metastable ground state product (**1b**). Steric interaction between the phenyl groups of the rotor and stator dictates that this motion occurs overwhelmingly in the "forward" direction (**1a** to **1b**). The metastable product (**1b**) lies slightly above the minimum energy and is separated from the true minimum energy geometry (**1c**) by a barrier on the ground state PES. This energy difference arises due to the absolute

Received: January 4, 2017
Revised: February 14, 2017
Published: February 20, 2017

DOI: 10.1021/acs.jpca.7b00087
J. Phys. Chem. A 2017, 121, 2138−2150

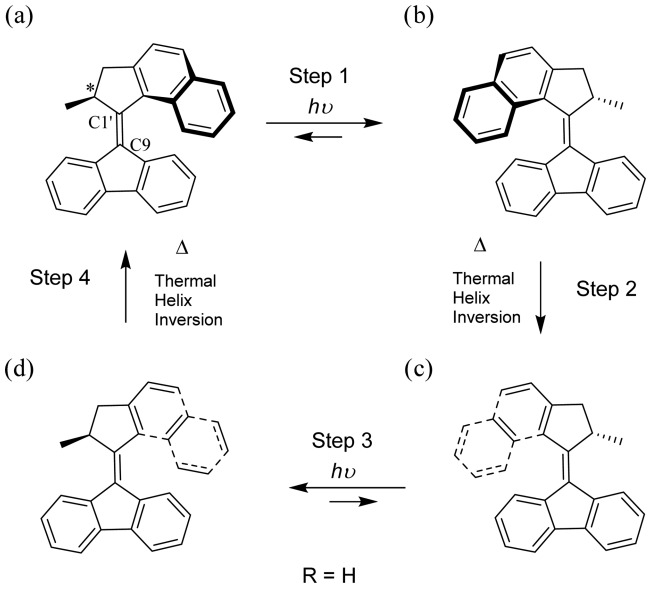

Figure 1. Mechanism of unidirectional rotation in a second-generation molecular motor. The "stable" ground state (**1a**) absorbs a photon and undergoes an excited state cis−trans isomerization to generate the "metastable" ground state product (**1b**). A ground state thermal helix inversion then generates the "stable" isomer (**1c**). Absorption of a second photon leads to a further cis−trans isomerization in the original direction to yield (**1d**) and a subsequent thermal helix inversion completes one full rotation (**1a**).

stereochemistry of the stereogenic center (* in **1a**, Figure 1). In the initial ground state structure (**1a**), the methyl group adopts the energetically favorable axial orientation. However, the metastable product of the isomerization reaction (**1b**) places this methyl group in the less energetically favorable equatorial orientation. As a result, **1b** undergoes a thermally activated helix inversion in which the methyl group is returned to the favorable axial conformation, and the full isomer product (**1c**) is formed. This reintroduces the steric barrier to isomerization in the reverse direction (**1c** to **1b**), meaning any subsequent excitation of the system results in overwhelming rotation in the "forward" direction to generate **1d**. Under constant irradiation, the system thus moves continuously around the cycle rotating selectively in the forward direction.

Since the initial overcrowded alkene design for unidirectional rotary molecular motors was first demonstrated,[11] significant progress has been made in developing refined systems with increasingly controllable properties. The first generation of molecular motors employed identical rotor and stator groups with two stereogenic centers.[12] A significant improvement in rotational speed and photochemical efficiency was found in the second generation design by incorporating distinct rotor and stator groups with a single stereogenic center.[13,14] More recently, a third generation design has been described in which two separate rotor units, connected to the central core of the molecule, rotate in unison in the same direction.[15] In the present study, we focus on the second generation of molecular motors (Figure 1 and Figure 2), building upon the existing work devoted to characterizing the motor dynamics of both the excited state isomerization[16,17] (step 1 in Figure 1) and ground state thermal helix inversion[18] (step 2 in Figure 1). Our initial report[16] on the excited state dynamics of **1** (Figure 2) revealed that the primary excited state process involves structural dynamics occurring on an exceptionally fast time scale (∼1 ps). A distinct bimodal fluorescence decay was observed, leading to the assignment of a two-coordinate mechanism for the excited state reaction. First, the initial Franck−Condon excited state relaxes in ca. 100 fs to a nonfluorescent local minimum on the excited state surface. From here, the population relaxes to the ground state via a conical intersection (CI) on a ∼ 1 ps time scale. The sensitivity of the excited state dynamics to both the electronic structure of the molecule and solvent viscosity were also investigated;[17] the initial relaxation from the Franck−Condon state was not sensitive to either, but the decay of the population from the local minimum

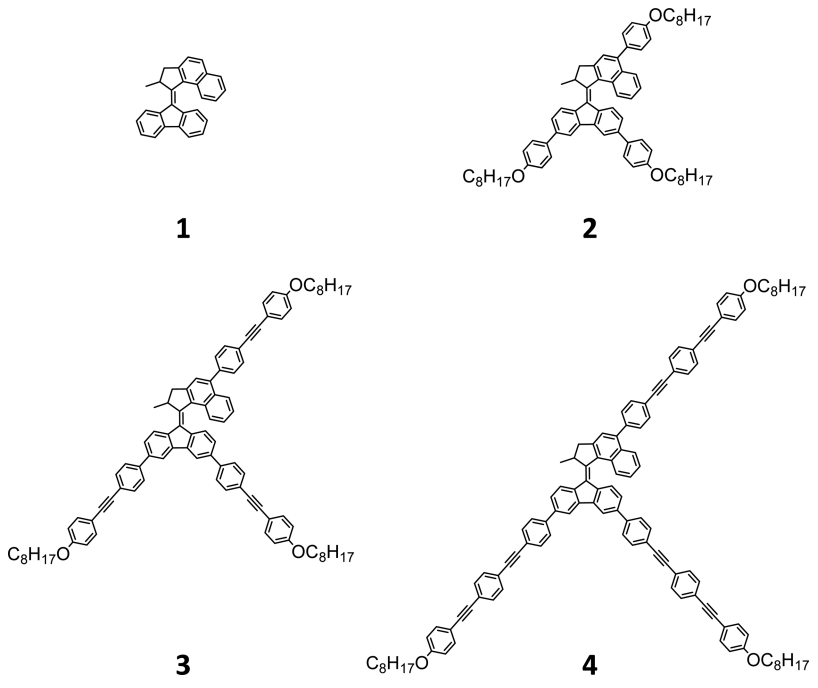

Figure 2. Parent molecular motor (**1**) and its derivatives substituted with phenyl (**2**) and poly(phenylethynylene) groups of increasing length (**3** and **4**).

DOI: 10.1021/acs.jpca.7b00087
J. Phys. Chem. A 2017, 121, 2138−2150

to the ground state exhibited a significant dependence upon both. This suggested the assignment of a volume conserving pyramidalization coordinate to the relaxation of the Franck−Condon state, and a twisting coordinate resulting in decay of the population from the local minimum to the original or the metastable ground states, the yield of the metastable state ultimately resting on the location and topology of the CI relative to the saddle point on the ground state surface.

In contrast to the excited state isomerization, the dynamics of the ground state thermal helix inversion in **1** are slow.[18] The half-life of the metastable state (1b in Figure 1) is ∼5 min, making the helix inversion the rate limiting step of the rotary cycle by several orders of magnitude. Electron donating and withdrawing substituents were found to have no significant impact upon the dynamics of the thermal helix inversion in **1**.[18] It was therefore concluded that steric (rather than electronic factors) are the primary factors controlling dynamics of the ground state process.

Recent attention has focused on the use molecular motors in functional applications. Ultimately, the goal is to form molecular machines, driving concerted motion with a large number of combined molecular motor units. Although this has not yet been achieved synthetically, several key applications of unidirectional molecular rotary motors have been demonstrated. These include functionalization of surfaces[19,20] and nanoparticles,[21] a molecular "nanocar",[22] and catalysis.[23] One particularly interesting potential application of the molecular motor system in nanoscience is as a molecular "stirrer bar".[24] If the rotational motion of the motor involves geometry changes which are large enough to displace a significant volume of solvent molecules, then there is potential for molecular motors to function as stirrers on the molecular scale. The extent to which the rotary mechanism requires solvent displacement was investigated by Chen et al.[24] Long, rigid substituents were added to a first-generation molecular motor structure and their effects on the dynamics of the ground state thermal helix inversion were measured. The rate of helix inversion was found to decrease significantly with both increasing substituent length and increasing solvent viscosity. Significantly, this viscosity dependence became stronger with longer substituents. It was concluded that long, rigid substituents significantly increased the rearranging volume associated with the rotary mechanism, leading to greater solvent displacement during rotation. This caused retardation of the thermal helix inversion as well as a substituent size dependent sensitivity to solvent viscosity.

Although the effect of long substituents upon the ground state dynamics has been characterized, no information was obtained regarding the impact of such substituents on excited state relaxation; in this paper we report on the effects of such long bulky substituents on the excited state dynamics of second generation unidirectional rotary motors. To do so, we consider derivatives of **1** substituted at three positions (two on the stator, one on the rotor) with phenyl (**2**) and phenylethynylene groups of increasing length (**3** and **4**, Figure 2). By probing the steady state spectroscopy and ultrafast fluorescence of each derivative, we determine the extent to which the excited state structural dynamics are retarded by these substituents. We also assess the sensitivity of the excited state dynamics to solvent viscosity. Finally, the dynamics of the ground state thermal helix inversion of **1**−**4** are studied. The rates of both the photochemical formation and thermal decay of the metastable state (**1b** in Figure 1) are probed as a function of substituent length. Chen et al.[24] previously reported the effect of substituent length on the rate of ground state helix inversion in a series of first generation molecular motors. The present study extends this to second generation motors (**1**−**4**, Figure 2).

RESULTS AND DISCUSSION

Steady State Spectroscopy. The steady state absorption and emission spectra for **1**−**4** recorded in dichloromethane (DCM) are shown in Figure 3. As described previously,[16,17] **1** exhibits a single band absorption spectrum attributed to an S_0-S_1 transition, localized on the "axle" double bond. In contrast, **2**−**4** exhibit dual band absorption spectra. The higher energy band grows in intensity and is increasingly red-shifted with increasing substituent chain length. This is consistent with experimental studies of poly(phenylethynylene) containing structures, where the maximum wavelength of absorption was found to increase with increasing polymer chain length,[25,26] an effect attributed to an extension of the delocalized π-electron system. Further calculations also suggested that the LUMO−HOMO band gap decreased with increasing poly(phenylethynylene) chain length in a series of silole-based oligomers.[27] Thus, we ascribe the higher energy bands in the absorption spectra of **2**−**4** to electronic transitions localized on the phenyl and phenylethynylene substituents. This assignment was confirmed by recording the

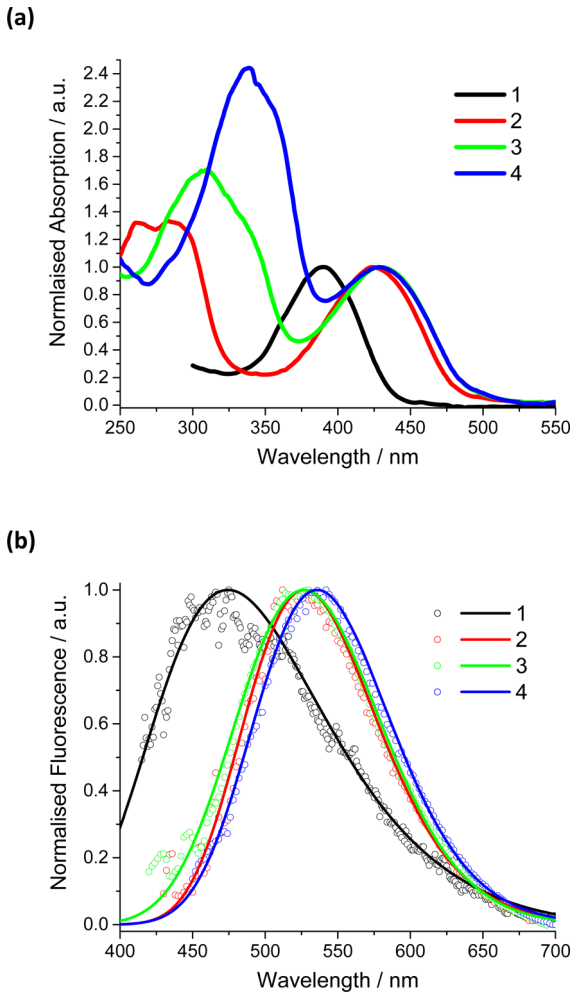

Figure 3. (a) Steady state absorption spectra of **1**−**4** recorded in dichloromethane (DCM). (b) Steady state fluorescence spectra of **1**−**4** recorded in DCM. Excitation was at the wavelength of maximum absorption in each case. Solvent Raman contributions were removed and the raw data (points) were fit to a log-normal function (lines).

DOI: 10.1021/acs.jpca.7b00087
J. Phys. Chem. A 2017, 121, 2138−2150

absorption spectra of the isolated phenylethynylene chains which overlap closely with the higher energy bands observed in the absorption spectra of **2**−**4**. (Supporting Information, Figure S1), although the spectra are broadened in the motors.

In comparison to **1**, the S_0−S_1 band in **2** exhibits a significant ∼25 nm red shift. However, increasing the length of the substituents further has a much smaller effect, with only a ∼5 nm red shift observed between **2** and **3**, and no difference at all between **3** and **4**. The red shift in the absorption is accompanied by an approximate doubling of the oscillator strength, from ca. 25000 M^{-1} cm^{-1} in **1** to ca. 50000 M^{-1} cm^{-1} in **2** and **3**. The fluorescence emission spectroscopy follows a similar pattern when excited near the maximum wavelength of the axle localized absorption (i.e., the lowest energy band). A significant ∼50 nm red shift is found for fluorescence of **2** compared to **1**, but increasing the substituent length further has a smaller effect, with a ∼ 14 nm red shift observed between **2** and **4** in dichloromethane (DCM). The large red shift in the absorption and emission maxima observed between **1** and **2**−**4** largely follow the trends observed previously for derivatives of **1** substituted with electron donating/withdrawing groups,[17] where substitution on **1** with methoxy (OMe), an electron donating group, shifted the absorption and emission maxima by ∼20 and ∼40 nm, respectively. This suggests that the substituents in **2**−**4**, as well as increasing the molecular volume, also act as weak inductive electron donors, donating electron density to the delocalized π system.

Steady state fluorescence spectra were also recorded on excitation at 400 nm (Supporting Information, Figure S2a), the excitation wavelength used for ultrafast fluorescence up-conversion. No excitation wavelength dependence was observed in the emission of **1**−**3**, but a large blue shift and increase in intensity was observed in **4** when excited at 400 nm compared to 430 nm. We ascribe this to a contribution to the emission from the phenylethynylene substituents which absorb at 400 nm in **4**. Phenylethynylene oligomers are strongly emissive in the 350−400 nm region, with fluorescence quantum yields of up to 0.93 reported.[28−30] In **4** the absorption of the longer phenylethynylene substituents is sufficiently red-shifted (Figure 3a) such that excitation occurs at 400 nm. The quantum yield of the phenylethynylene emission is larger than that of the motor unit,[16,28] leading to the intense blue-shifted emission. Thus, excitation of **4** at 400 nm results in emission from both the core unit of the motor and the phenylethynylene substituents, while only emission from the core unit is observed in **2** and **3** under the same conditions. As a result, ultrafast fluorescence of **4** was not measured, as the optimum excitation wavelength for that experiment is 400 nm.

The solvent dependence of the electronic spectra were also recorded, with peak wavelengths collected in Table 1. As reported in our previous studies of **1**,[16,17] the absorption maxima of **2**−**4** showed no significant dependence upon solvent polarity, and the substituent dependence of the absorption spectra described above for **1**−**4** in DCM was retained in each solvent studied.

Finally, the relative fluorescence quantum yields of the core unit localized emission in **1**−**4** were compared. The fluorescence quantum yields of **1**−**4** are all low, but vary significantly. Figure 4 shows the steady state fluorescence spectra of **1**−**4** in octanol normalized to the absorbance at the excitation wavelength (wavelength of maximum absorption) in each case, i.e. the relative fluorescence quantum yield. Two important features are revealed. First, derivatives **2**−**4** are significantly more fluorescent than **1**. Second, no increase is found in the emission intensity of **3** compared to **4** despite the increase in substituent length between the derivatives. Thus, the addition of substituents to **1** leads to an enhancement in fluorescence, but the effect of length or volume of the substituent itself is slight. This result is investigated more thoroughly via ultrafast fluorescence spectroscopy (below).

Table 1. Absorption and Emission Wavelength Maxima of 1−4

	absorption maximum wavelength/nm			
	1	**2**	**3**	**4**
isopentane	–	415	422	427
DCM	406	424	429	429
cyclohexane	402	420	424	423
decalin	403	422	426	427
ethanol	402	420	422	435
butanol	–	421	426	428
octanol	404	422	428	428
decanol	–	422	425	429
	emission maximum wavelength/nm			
	1	**2**	**3**	**4**
isopentane	–	519	510	616
DCM	475	522	528	536
cyclohexane	489	520	520	528
decalin	508	520	523	528
ethanol	470	522	534	–
butanol	–	521	522	591
octanol	472	519	528	612
decanol	–	522	521	610

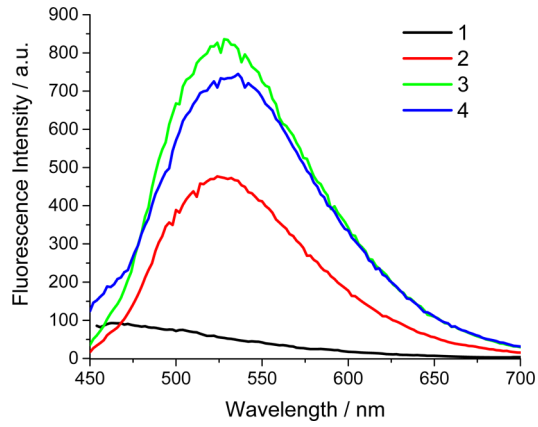

Figure 4. A relative measurement of the fluorescence quantum yields of **1**−**4** in DCM. In each case, excitation was at the respective wavelength of maximum of absorption and emission intensity was corrected for absorption intensity at this wavelength.

Substituent Dependent Ultrafast Fluorescence. The fluorescence decay data for **1**−**3** measured in DCM are shown in Figure 5. Several features are shared with our previous reports on **1** and its derivatives.[16,17] The decay of all samples are ultrafast, non-single exponential and exhibit oscillatory features due to coherent vibrational dynamics in the excited state. As reported previously for **1**,[16] a significant emission wavelength dependence is also observed for **2** and **3**, where tuning the emission wavelength to the red leads to an increased mean excited state lifetime (Supporting Information, Figure S3). This corresponds to an ultrafast red shift in the emission of **1**−**3** and has been discussed in detail elsewhere for this molecular motor system.[17] Despite these similarities, Figure 5 reveals some striking

DOI: 10.1021/acs.jpca.7b00087
J. Phys. Chem. A 2017, 121, 2138−2150

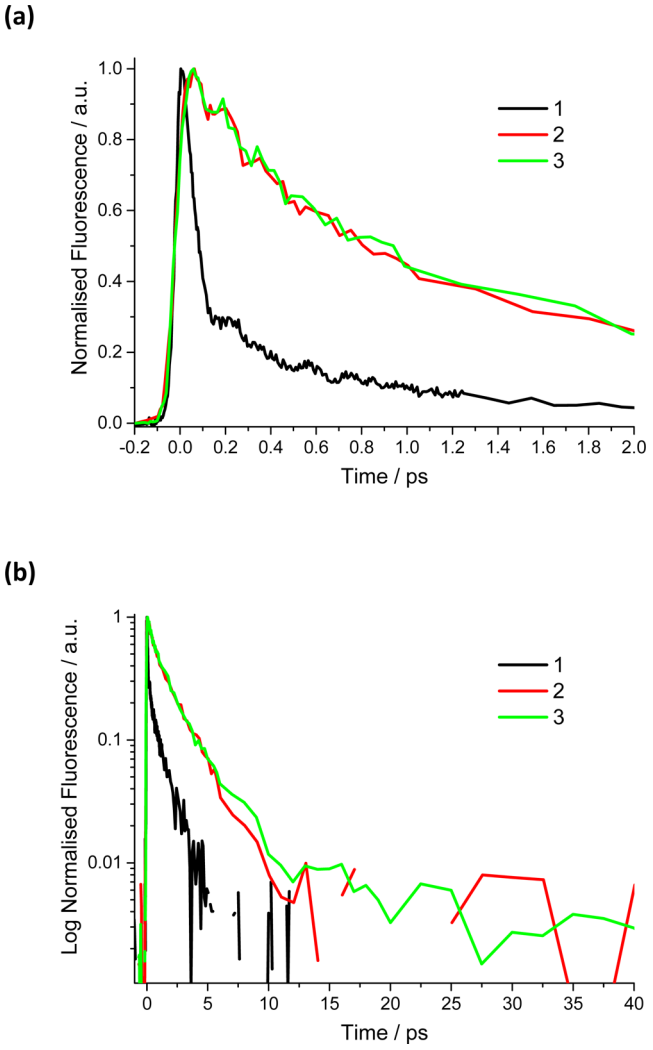

Figure 5. Fluorescence up-conversion data for **1**−**3** in DCM recorded at an emission wavelength of 540 nm after excitation at 400 nm. Low frequency oscillations are due to coherent dynamics in the excited state: (a) first 2 ps after excitation on a linear intensity scale and (b) first 40 ps after excitation on a log intensity scale.

differences between **1** and **2**−**3**. On the fastest time scale (Figure 5a), it is clear that the decay in **2** and **3** is not dominated by the large amplitude extremely fast ∼100 fs component observed in **1**. Further, examination of the longer time scale data (Figure 5b) reveals that components of the emission of **2** and **3** are significantly longer lived compared to **1**. A further striking observation arises when comparing the decay dynamics of **2** and **3**. Despite the substantial increase in substituent size from **2**-**3**, the decay curves of each derivative in DCM are remarkably similar. Thus, as was noted in the electronic spectra, the effect of substitution on **1** is large, specifically a decreased amplitude of the very fast relaxation from the FC state and an overall longer lifetime; however, the effect of further increasing substituent size from **2** to **3** is modest.

All the time-resolved fluorescence data were fit to sums of exponentially decaying components. In our previous study,[16] we reported that the excited state population of **1** was well described by a three term exponential decay function plus oscillatory components. The oscillatory components arise from coherently excited vibrational modes in the electronic excited state modulating both the energy of the excited state and its transition moment to the ground state.[31−33] These modes are damped on a sub picosecond time scale. In this study, we focus on the population dynamics, and do not discuss the coherent vibrational dynamics further. In order to exclude any effect of the rapidly damped oscillatory components on the analysis of the population decay data, the first 200 fs of each decay curve were excluded from the fitting procedure. Under these conditions the fluorescence decay data for **2** and **3** in DCM were well fit by a sum of three exponential terms; the full results of the fitting procedure for **2** and **3** and previously published results for **1** in DCM are collected in Table 2.

Table 2. Fluorescence Lifetime Data for 1−3 in DCM

derivative	τ_1/ps	A_1	τ_2/ps	A_2	τ_3/ps	A_3	$\langle\tau\rangle$/ps
1	0.08	0.77	0.32	0.16	1.02	0.07	0.18
2	0.10	0.44	0.70	0.24	2.44	0.32	1.00
3	0.16	0.36	1.47	0.54	4.81	0.10	1.33

Substituents affect the average fluorescence lifetimes ($\langle\tau\rangle$). Compared to **1**, the smallest phenyl substituent (**2**) results in a greater than 5 fold increase in $\langle\tau\rangle$. However, increasing the size of the substituents further has a comparatively minor effect, with an increase of only 30% between **2** and **3**. Additional effects of substitution are revealed in the individual lifetimes. Although the time constant of the fastest term (τ_1) shows only a minor substituent dependence (a 2-fold increase from **1** to **3**), its amplitude (A_1) decreases by a factor of 2 between **1** and **2**−**3**. Thus, τ_1 is the dominant decay term (∼80%) in **1** while it contributes only 40% of the amplitude in **2** and **3**; this is also evident in Figure 5a. Comparing τ_2 and τ_3 for **1**, **2**, and **3** reveals that both time constants are similar in **2** and **3** but are both longer than that in **1**. The ultrafast relaxation time (τ_1) was assigned to a volume conserving pyramidalization at an axle carbon atoms, leading to a nonemissive "dark" region on the excited state surface.[16,34−36] Very recently Pang et al. extended excited state calculations on **1** to accurately simulate the ultrafast fluorescence measurements.[37] They reported that progress to the dark state occurs mainly via a ca. 40° degree bond rotation, with pyradmidalization required to reach the CI. The large twist of two relatively large groups through the solvent seems at odds with the observed viscosity independence. However, the calculation also suggests that fluorescence might be quenched at smaller angles of the twist coordinate, and that other coordinates are involved which may combine to yield a volume conserving coordinate, as the experiment requires.[37] The data for **2** and **3**, where even the largest substituents result in only a minor increase in τ_1, show that bulky substituents on the periphery of the molecule do not retard this essentially localized intramolecular motion.

It was previously shown that τ_2 and τ_3 exhibit a sensitivity to the electron donating/withdrawing character of the substituents. These longer relaxation times were ascribed to the decay of the excited state population from the nonemissive local minimum on the excited state potential surface, where the dark state is in thermal equilibrium with the emissive Franck−Condon state. In this model the longer decay components reflect the decay of the dark state back to the electronic ground state via a CI.[16,17] Experiment and theory suggested that this decay occurred via motion along a coordinate involving a larger scale molecular motion, most likely torsion about the central axle bond. The present data reveal two features regarding these new substituents. First, the larger amplitude of τ_2 and τ_3 in **2** and **3** may arise from a

DOI: 10.1021/acs.jpca.7b00087
J. Phys. Chem. A 2017, 121, 2138−2150

smaller energy difference between bright and dark states, giving rise to a larger thermal population in the emitting state; this is also consistent with a higher fluorescence quantum yield for these derivative (Figure 4). However, it was noted above that the oscillator strength for **2** and **3** is twice that of **1**. If this is reflected in the $S_1 \rightarrow S_0$ transition moment then that may also enhance the amplitude of the long component in the bright state emission. Thus, even though the amplitude is significantly increased it may not point to a significant change in energy gap between bright and dark states on the excited state potential energy surface. The dependence on substituent volume observed in τ_2 and τ_3 (**1** compared to **2**) could also be consistent with a twisting coordinate. However, such an assignment is not consistent with the relatively small effect observed upon further increasing the length of the substituent (i.e., **2** compared to **3**). The solvent displacing torsional coordinate is expected to be sensitive to both the volume of the molecule twisting about the central bond and the solvent viscosity; this apparent inconsistency is studied further through the solvent viscosity dependence.

Solvent Dependent Ultrafast Fluorescence. An important probe of excited state dynamics in the condensed phase is the solvent polarity and viscosity dependence. Solvent polarity effects highlight substantial changes in charge transfer character between electronic states. On the other hand, molecular motions displacing large volumes of solvent are expected to be resisted in viscous media. Both effects will be reflected in solvent dependent excited state spectra and dynamics. A total of eight solvents were investigated with a view to distinguishing polarity and viscosity dependencies in **1**−**3**. The solvents ranged in polarity from ethanol ($\varepsilon_r = 25$) to cyclohexane ($\varepsilon_r = 2$) and in viscosity from ethanol ($\eta = 1.07$ m Pa s^{-1}) to decanol ($\eta = 10.9$ m Pa s^{-1}) for alcohol solvents and isopentane ($\eta = 0.214$ m Pa s^{-1}) to decalin ($\eta = 2.5$ m Pa s^{-1}) for nonpolar solvents. Alcohols are a useful solvent series for viscosity dependent studies, as large changes in viscosity can be made without dramatically altering chemical properties of the solvent, such as H-bonding. Therefore, the viscosity dependence in alcohol solvents and nonpolar solvents will be considered separately. An example of solvent dependent fluorescence decay data is shown for derivative **2** in alcohol solvents (Figure 6a) and nonpolar solvents (Figure 6b). The corresponding data for derivative **3** are shown in Supporting Information (Figure S4). The decay data for each derivative were again fit to multiexponential decay functions as described for DCM above. Two exponential terms were adequate for the data recorded in isopentane, while three exponential terms were required for all other solvents. The fit parameters obtained for **1**−**3** in each solvent are summarized in Table 3.

In studying the viscosity dependence of the fluorescence decay dynamics in **2**−**3**, two key considerations must be made. First, are the dynamics slowed in viscous solvents? Second, does the lack of a significant dependence upon substituent length (i.e., the relatively minor differences between the decay of **2** and **3** in DCM) persist in all solvents? The time constants and calculated mean fluorescence lifetimes ($\langle\tau\rangle$) of **2** and **3** (Table 3) are represented by scatter plots in Figure 7a (alcohol solvents) and Figure 7b (nonpolar solvents). From these, it is apparent that the fluorescence decay dynamics of **2** and **3** exhibit a significant viscosity dependence. Qualitatively, the fluorescence decay slows with increasing viscosity in both alcohol and nonpolar solvents. The mean fluorescence lifetimes for both **2** and **3** increase by a factor of ∼4 between the lowest and highest viscosity solvents for both alcohol and nonpolar solvents.

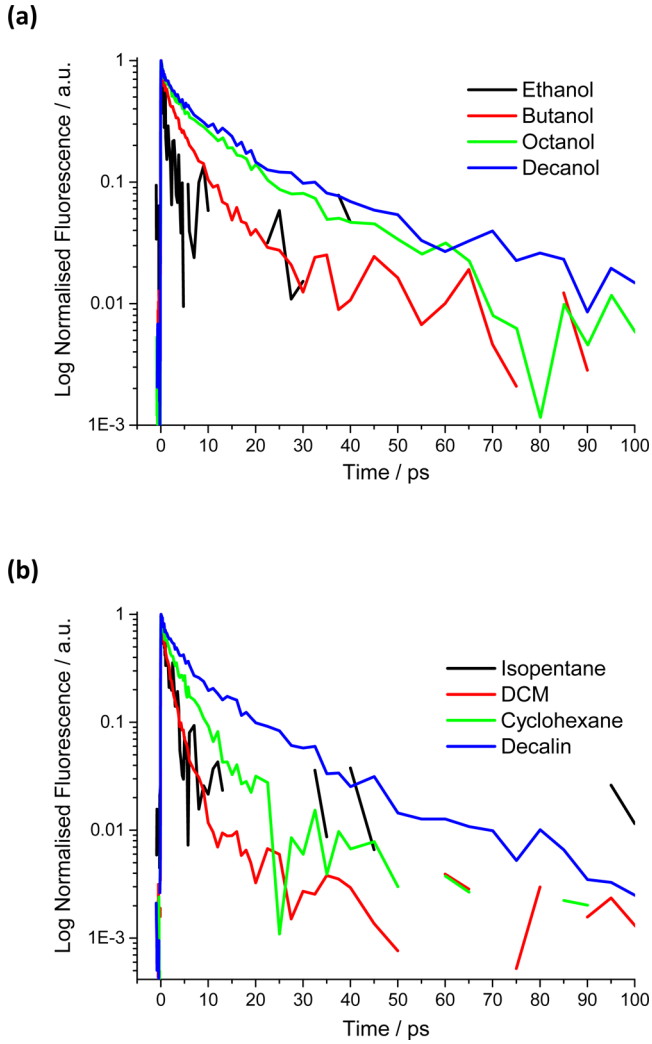

Figure 6. Fluorescence up-conversion data for **2** recorded as a function of solvent viscosity. Emission was recorded at 540 nm after excitation at 400 nm. (a) Polar alcohol solvents and (b) nonpolar solvents.

Turning to the individual time constants, the most significant viscosity dependence is found for the longest component (τ_3) (Figure 7). The τ_3 values recovered for **2** and **3** in alcohol solvents exhibit a ∼4 fold increase over the viscosity range studied. A similar trend is observed in nonpolar solvents whereby **2** exhibits a ∼ 5 fold increase and **3** a ∼6 fold increase over the viscosity range measured. A similar but smaller effect is observed for the intermediate time constant, τ_2. Finally, the shortest exponential term (τ_1) shows the weakest viscosity dependence. In alcohol solvents, τ_1 shows no sensitivity to viscosity within experimental error over the entire viscosity range for all three derivatives. In nonpolar solvents, a ∼2 fold increase is observed for **2** and **3**. The very weak viscosity dependence of τ_1 in **2** and **3** across all solvents studied is consistent with a volume conserving pyramidalization (or small angular rotation) coordinate. The significant viscosity dependence found for τ_2 and τ_3 is consistent with the larger scale, solvent displacing coordinate (such as twisting about the central double bond) assigned to these time constants.

Having established a clear viscosity dependence in the fluorescence decay dynamics of **2** and **3**, the relationship between solvent friction and substituent length will be considered. Qualitatively, the data recorded in each solvent

DOI: 10.1021/acs.jpca.7b00087
J. Phys. Chem. A 2017, 121, 2138−2150

Table 3. Viscosity dependent Lifetime Data for 1−3.

	derivative **1**				
	nonpolar solvents			alcohol solvents	
	DCM	cyclohexane	decalin	ethanol	octanol
A_1	0.77	–	0.70	–	0.66
τ_1/ps	0.08	–	0.07	–	0.12
A_2	0.16	0.75	0.18	0.77	0.27
τ_2/ps	0.32	0.10	0.44	0.16	0.62
A_3	0.07	0.26	0.11	0.23	0.07
τ_3/ps	1.02	1.11	2.92	0.96	2.68
$\langle\tau\rangle$/ps	0.18	0.36	0.46	0.34	0.44

	derivative **2**							
	nonpolar solvents				alcohol solvents			
	isopentane	DCM	cyclohexane	decalin	ethanol	butanol	octanol	decanol
A_1		0.44	0.11	0.13	0.33	0.32	0.23	0.25
τ_1/ps		0.10	0.25	0.24	0.13	0.15	0.25	0.15
A_2	0.44	0.24	0.26	0.49	0.38	0.30	0.39	0.29
τ_2/ps	0.73	0.70	1.03	3.10	1.20	1.39	3.18	2.10
A_3	0.56	0.32	0.63	0.38	0.29	0.38	0.38	0.46
τ_3/ps	2.41	2.44	4.48	12.32	4.44	6.70	17.35	16.49
$\langle\tau\rangle$/ps	1.66	1.00	3.12	6.20	1.79	2.98	7.83	8.24

	derivative **3**							
	nonpolar solvents				alcohol solvents			
	isopentane	DCM	cyclohexane	decalin	ethanol	butanol	octanol	decanol
A_1		0.36	0.29	0.24	0.17	0.26	0.15	0.26
τ_1/ps		0.16	0.34	0.33	0.15	0.28	0.22	0.16
A_2	0.45	0.54	0.17	0.45	0.59	0.38	0.38	0.33
τ_2/ps	0.70	1.47	1.34	3.80	1.09	2.31	2.47	2.97
A_3	0.55	0.10	0.54	0.31	0.24	0.36	0.48	0.42
τ_3/ps	2.54	4.81	5.12	16.89	5.01	7.72	15.66	19.45
$\langle\tau\rangle$/ps	1.72	1.33	3.09	7.02	1.88	3.70	8.47	9.13

reproduce the lack of a significant substituent size dependence observed for DCM. In each solvent studied, the mean fluorescence lifetime ($\langle\tau\rangle$) is insensitive within experimental error to the length of the phenylethynylene substituents (Table 3 and Figure 7). Thus, although the excited state lifetime is increased by substitution of **1** with phenyl groups (**2**), it does not increase further with further increases in the substituent length (**2** compared to **3**), even in the most viscous solvents. This is a surprising result. The phenylethynylene unit is generally considered a rigid one so a complete torsional motion in the isomerization reaction would lead one to predict that an increased volume of solvent must be displaced between **2** and **3**. This is evidently not the case—the increasing volume effect has already saturated by **2**. However, it is important to note that what is being probed by time-resolved fluorescence is not necessarily the complete rotation about the axle, but only that motion required to reach the CI where population decays to the ground state. It may be that a much smaller scale twist is required to promote internal conversion, which does not require the motion of the large substituents through the solvent. Indeed it is plausible that the pathway to the CI is modified when substituents are large and the medium is viscous. This would require the existence of alternative low barrier pathways to the CI on the multidimensional excited state potential, which might, in line with some recent calculations, also involve the pyramidalization coordinate.[37] Such effects might be probed by finer control over the volume displaced by the coordinate and particularly by refined excited state dynamics calculations.

Although the longer decay times scale consistently with viscosity (Figure 7), a possible role for solvent polarity should also be considered. Polarity effects may be significant if there are appreciable changes in molecular dipole moment during motion along (or transitions between) potential energy surfaces, e.g. between the Franck−Condon and "dark" states. Unfortunately the low solubilities of the present solutes in polar non H-bonding solvents precluded a detailed investigation of solvent polarity, but good quality data were obtained in cyclohexane and ethanol, which have very similar viscosities (≈1 cP) but very different polarities (ε_r = 2 and 24 respectively). The mean relaxation time $\langle\tau\rangle$ for both **2** and **3** is longer (by approximately a factor of 2) in cyclohexane than in ethanol, suggesting a small polarity effect. However, analysis of the individual decay times reveals that τ_2 and τ_3 are very similar in cyclohexane and ethanol for both **2** and **3**, distinguishing this from the viscosity dependence (Figure 7). From this, we conclude that the solvent dependence of these longer decay times indeed arises from the solvent viscosity effect (Figure 7). This is consistent with radiationless decay along a torsional coordinate being opposed by solvent friction. However, that coordinate must involve a more local reorganization than complete rotation of the rotor part of the molecule. On the other hand the largely viscosity independent τ_1 is observed to be consistently longer in cyclohexane than in ethanol. This raises the possibility that the fast relaxation out of the Franck−Condon state, assigned to a volume conserving pyramidalization coordinate, is sensitive to solvent polarity in **2** and **3**. However, the data in the less viscous but only slightly polar solvent DCM

DOI: 10.1021/acs.jpca.7b00087
J. Phys. Chem. A 2017, 121, 2138−2150

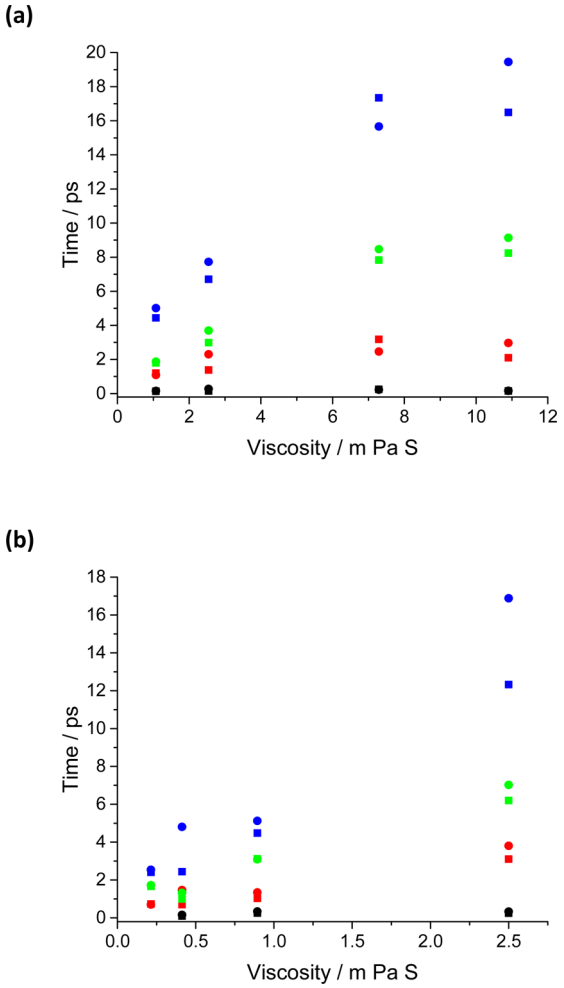

Figure 7. A summary of the exponential time constants τ_1 (black), τ_2 (red), τ_3 (blue), and average fluorescence lifetime $\langle\tau\rangle$ (green) fit to the fluorescence decay data of **2** (squares) and **3** (circles) as a function of solvent viscosity in (a) polar alcohol solvents and (b) nonpolar solvents.

($\varepsilon_r = 9$) shows an even faster τ_1 than in ethanol; this suggests that the demonstration of a polarity effect on τ_1 requires a more detailed study in solvents of a range of polarities at fixed viscosities—i.e. an isoviscosity analysis.

Ground State Thermal Helix Inversion. Having established that substitution of **1** with phenyl and poly(phenylethynylene) groups does slow down the excited state reaction, but that increasing the length of these substituents further has little additional effect, we here consider the role of substituent size upon the rate of the ground state thermal helix inversion (step 2 in Figure 1). A previous study by Chen et al.[24] concluded that substitution on the rotor and stator of a first generation molecular motor with alkyl substituents of increasing size resulted in increased retardation of the thermal helix inversion. However, the second-generation molecular motor described in the present study has a substantially different design of its core molecular structure compared to first generation motors. This is an important consideration, since the rotary mechanism and dynamics of overcrowded alkene molecular motors are highly sensitive to molecular structure.[13] Here, we extend the study of the effects of substituent volume and medium viscosity on ground state thermal helix inversion to the second generation molecular motors shown in Figure 2. Our aims were first to determine whether the phenyl and phenylethynylene substituents resulted in retardation of thermal helix inversion (**1** compared to **2**–**4**) and second whether increasing the length of substituents resulted in increased retardation.

1–**4** were first optically pumped to their respective photostationary states to generate the maximum concentration of the metastable state (**1b** in Figure 1). The relaxation time of this population to the product isomer (**1c** in Figure 1) was then recorded in each case as a function of substituent, solvent viscosity and temperature. The viscosity dependent measurements were conducted in the same series of solvents described above, while a temperature dependent study was performed in cyclohexane at temperatures ranging from 10 to 60 °C. Separation of the metastable and product forms (**1b** and **1c**, respectively, in Figure 1) of the molecular motor is possible since the electronic absorption maxima of **1**–**4** exhibit a significant red shift (~30 nm) between these two forms. Furthermore, due to the symmetric nature of the molecular structure in **1**–**4**, the initial structure and product isomer (1a and 1c respectively in Figure 1) of each derivative are identical. As an example, Figure 8

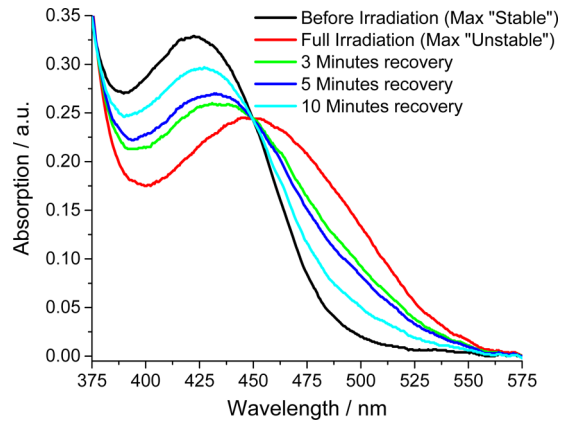

Figure 8. Absorption spectra of **2** in cyclohexane as a function of recovery time after irradiation at 405 nm. Prior to irradiation (black line), the spectrum represents only the initial state (1a, Figure 1) population. After 20 min irradiation (red line), the spectrum represents a mixture of the initial and metastable state (**1a** and **1b** respectively, Figure 1) populations at the photostationary state. After the lamp was switched off (green, blue, and cyan lines), the metastable population relaxes to the product isomer (1c, Figure 1) and the original absorption spectrum is recovered.

shows the absorption spectra of **2** in cyclohexane before irradiation (**1a** in Figure 1), at the photostationary state under constant irradiation (maximum concentration of metastable form, **1b**) and at several time intervals after irradiation (showing relaxation of metastable **1b** to product **1c**). Figure 8 shows that the red-shifted portion of the absorption spectrum can be attributed to the metastable population. For each derivative, solvent and temperature studied, the relaxation of the metastable population was recorded by integration of the area of the spectrum between 470 to 500 nm as a function of time, with the relaxation at room temperature occurring in several minutes. Examples of the decay curves as a function of substituent and temperature are shown in Figure 9. All decay curves were well fit by a single exponential function to yield the relaxation time and hence the first order rate constant. The data are displayed in Tables 4 and 5. Figure 10 summarizes on a single plot both the viscosity dependence ($\ln k$ vs η on the upper y-axis) and temperature dependence ($\ln k$ vs $1/T$ on the lower y-axis) for **1**–**4**. From Figure 10, it is immediately apparent that the rate of

DOI: 10.1021/acs.jpca.7b00087
J. Phys. Chem. A 2017, 121, 2138–2150

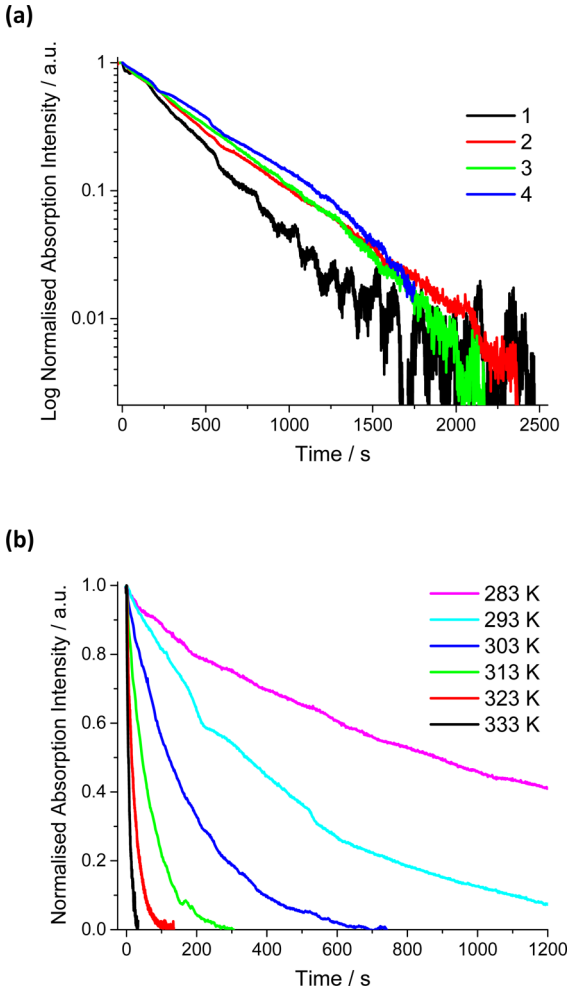

Figure 9. Integrated intensity of absorption (470 to 500 nm) in cyclohexane recorded as a function of time. This spectral region can be solely attributed to the metastable population (**1b**, Figure 1), and thus shows the time domain relaxation of this population via the thermal helix inversion. (a) **1**−**4** in cyclohexane recorded at 20 °C. (b) **2** in cyclohexane as a function of temperature.

relaxation in **1**−**4** is independent of solvent viscosity but exhibits a significant dependence upon temperature.

This result can be interpreted by application of a free volume model,[38] a modification of the Kramers equation. This model has previously been applied to explain the viscosity dependence of several molecular systems in which rotational motion is involved,[38−41] including thermal helix inversion in a first generation molecular motor system.[24] Typically, the molecular rearrangement which facilitates such molecular motion involves only a portion of the molecule. As a result, the volume required to complete the rearrangement is a fraction of the total molecular volume. It is established that the thermal helix inversion proceeds via a thermally activated barrier crossing on the ground state potential energy surface.[11] In this case, the free volume model relates the rate constant (k) of the thermal helix inversion to the fractional molecular volume (α), medium viscosity (η) and activation energy (E_a) as follows:

$$k \propto \left(\frac{1}{\eta}\right)^{\alpha} e^{-E_a/RT} \quad (1)$$

The absence of a viscosity effect in **1**−**4** suggests a fractional volume for the molecular rearrangement (α) close to zero. Instead, it is the activation energy (E_a) which controls the relaxation rate constant. Thus, the thermal helix inversion in motors **1**−**4** is activation rather than viscosity controlled; it is the accumulation of energy in the reaction coordinate which determines the relaxation rate, not the medium friction. Table 6 summarizes the calculated activation energies for **1**−**4** in cyclohexane and shows that the activation energies are also independent of substituent within experimental error. Thus, the thermal barrier and hence rate of thermal helix inversion in this molecular motor system is not sensitive to the phenyl and poly(phenylethynylene) substituents.

The insensitivity of the thermal helix inversion rate constant to both solvent viscosity and substituent length is in contrast to the previous study of first generation molecular motors, where ground state dynamics were found to be a function of both substituent size and solvent viscosity.[24] Although the substituents on the two molecular motors are slightly different, they both consist of the rigid phenylethynylene unit. Thus, the difference between the data of Chen et al.[24] and that in Tables 4 and 5 points to a mechanistic difference between the ground state reaction pathways for first and second generation molecular motors. In fact it is already established that the molecular dynamics and kinetics in the ground state are extremely sensitive to the core structure of the molecular motor.[42] For example, the half-life of the metastable state in first generation molecular motors is between 25 and 40 times longer than those in the present study.[24] It is possible that the substantial modifications to the core structure between the two generations has resulted in significantly altered reaction pathways. Evidently, in the second generation motors studied here, it is the local reorganization in the core which controls the rate of helix inversion, and this appears to be independent of motor substituent size and medium viscosity; the activation barrier dominates the kinetics. In this connection, it would be particularly interesting to study the

Table 4. Viscosity Dependent Metastable State Lifetime Data and Calculated Rates of Ground State Thermal Helix inversion for 1−4, Measured at 20 °C

		1		2		3		4	
solvent	η/cP	τ/s	$k \times 10^3$/s^{-1}	τ/s	$k \times 10^3$/s^{-1}	τ/s	$k \times 10^3$/s^{-1}	τ/s	$k \times 10^3$/s^{-1}
isopentane	0.21	–	–	230	4.35	276	3.62	–	–
DCM	0.41	215	4.65	311	3.22	440	2.27	448	2.23
cyclohexane	0.89	299	3.34	330	3.03	408	2.45	387	2.58
decalin	2.50	–	–	340	2.94	274	3.65	323	3.10
ethanol	1.07	297	3.37	413	2.42	303	3.30	–	–
butanol	2.54	–	–	457	2.19	425	2.35	–	–
octanol	7.29	251	3.98	427	2.34	459	2.18	355	2.82

DOI: 10.1021/acs.jpca.7b00087
J. Phys. Chem. A 2017, 121, 2138−2150

Table 5. Temperature Dependent Metastable State Lifetime Data and Calculated Rates of Ground State Thermal Helix Inversion for 1−4 in Cyclohexane

	1		2		3		4	
temp/K	τ/s	$k \times 10^3$/s^{-1}	τ/s	$k \times 10^3$/s^{-1}	τ/s	$k \times 10^3$/s^{-1}	τ/s	$k \times 10^3$/s^{-1}
283	720	1.39	1414	0.71	809	1.24	1280	0.78
293	300	3.33	460	2.17	479	2.09	528	1.89
303	120	8.31	162	6.17	184	5.43	194	5.15
313	39.8	25.13	55.2	18.13	63	15.89	59.4	16.83
323	18.9	52.91	22.5	44.40	24.2	41.27	23.1	43.37
333	5.6	178.57	10.1	99.40	8.51	117.54	7.7	129.87

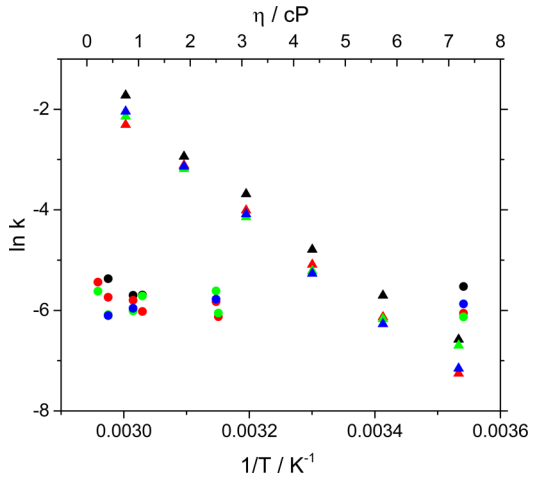

Figure 10. Rate of thermal helix inversion as a function of temperature (triangle symbols, bottom *x*-axis) and solvent viscosity (circle symbols, top *x*-axis) for **1** (black), **2** (red), **3** (green), and **4** (blue).

Table 6. Calculated Activation Energies for 1-4 in Cyclohexane

derivative	E_a/kJ mol^{-1}
1	75.2
2	78.2
3	73.1
4	80.8

excited state dynamics of first generation molecular motors; such measurements are planned.

Photochemical Rates of Formation of the Metastable State. Having concluded that the rate of decay of the metastable population (via thermal helix inversion) is insensitive to substituent length, we investigated the effects of substituent size upon the rate of ground to metastable state photoconversion. As described above, the absorption spectrum of the metastable state exhibits a ∼30 nm red shift compared to the ground state isomers (1a and 1c in Figure 1). Thus, as shown in Figure 11a, absorption in the 490−520 nm region provides an unambiguous separation of the metastable population (dashed lines) for **1**−**4**. For each derivative, the rate of formation of the metastable population was determined by simultaneously irradiating the sample with a 405 nm light emitting diode and recording the integrated absorption between 470 nm-500 nm (shaded area in Figure 11a) as a function of time. Figure 11b shows the time-resolved traces recorded for **1**−**4** in cyclohexane. Each trace was fit to a single exponential function to recover a first order rate constant as summarized in Table 7.

Two key features are apparent. First, the formation rate of the mestastable state is retarded by the substituents (**1** compared to

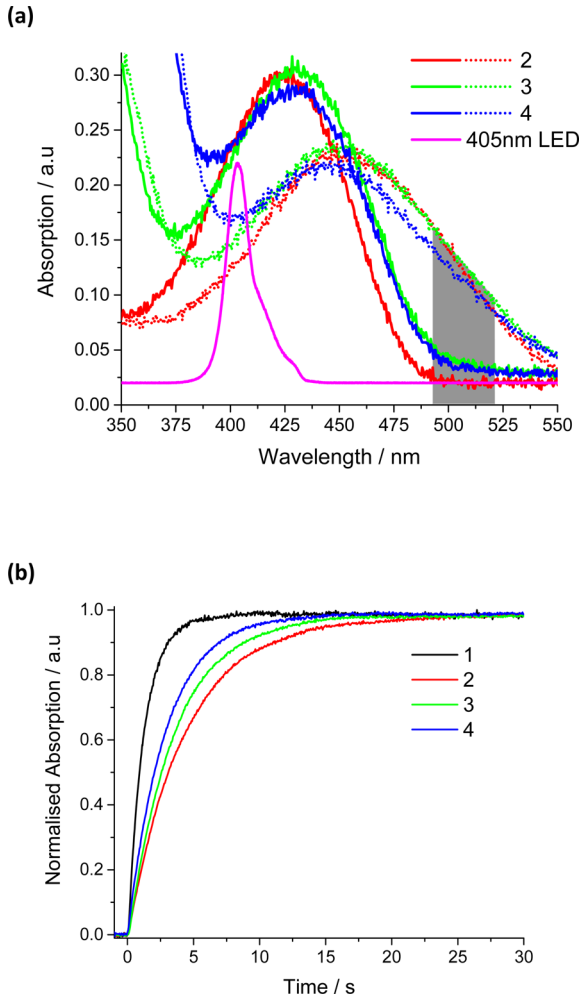

Figure 11. Formation of the metastable state of **1**−**4** in DCM. (a) Absorption spectra of the initial forms (solid lines) and metastable state products (dotted lines) of **1**−**4**, overlaid with the lamp spectrum used for excitation. The shaded box shows the spectral region over which the integrated intensity of absorption was recorded as a function of time. (b) Time-resolved integrated intensity of absorption measured between 470 and 500 nm for **1**−**4**.

Table 7. Exponential Rise and Calculated Rates of Formation of the Metastable State for 1−4 in DCM

derivative	τ/s	k/s^{-1}
1	1.23	0.81
2	4.51	0.22
3	3.63	0.28
4	2.9	0.34

DOI: 10.1021/acs.jpca.7b00087
J. Phys. Chem. A 2017, 121, 2138−2150

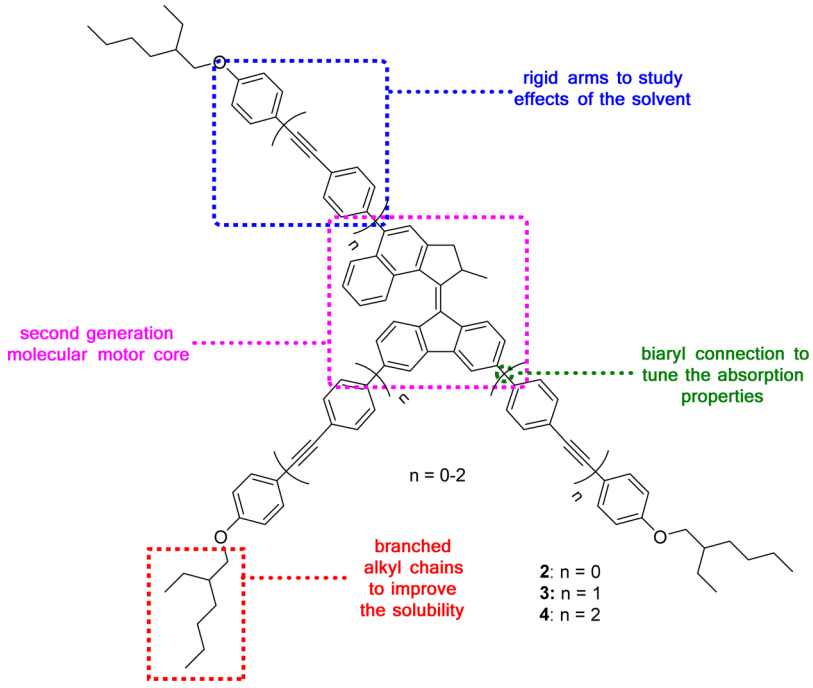

Figure 12. Design of the rigid-arm substituted molecular motors **2**−**4**.

2−**4**). This follows the trends established in the ultrafast excited state and thermal helix inversion studies described above. Second, of the three substituted derivatives, the largest substituents (**4**) exhibit the fastest formation rate while the smallest substituents (**2**) exhibit the slowest formation rate. This is a surprising result in the sense that the decay from the Franck−Condon state and the thermal helix inversion studied above are both independent of substituent size. However, those measurements probed different regions of the potential energy surface when compared to these photoconversion quantum yield data. The quantum yield of the metastable state will be influenced by two related features: the location of the CI coupling excited and ground states relative to the transition state on the ground state surface and the partitioning between the metastable and original ground states immediately after internal conversion. Which of these factors gives rise to the observed substituent dependence is not clear for the present study. Transient absorption experiments may be informative.

CONCLUSION

A detailed study of the kinetics of second generation molecular motors has been made as a function of the size of substituents added to the periphery of the molecule. Each motor was studied as a function of solvent viscosity to probe how motor kinetics, molecular volume and medium friction are coupled. As previously reported all solutes exhibit a biphasic excited state decay assigned to a two coordinate excited state reaction. We find that the slower component of that decay is viscosity dependent, consistent with a torsional motion about the "axle" of the motor. However, the viscosity dependence was shown to be independent of the size of the substituent. This suggests that the pathway leading to decay from the excited states (and ultimately to the changed ground state conformer (Figure 1)) is dominated by structure changes in the core of the motor, which do not involve large scale reorientation of the motor and its substituents.

We extended this study to the ground state thermal helix inversion reaction, which occurs 14 orders of magnitude more slowly than the excited state reaction. The rate of this reaction was found to be dominated by the thermal barrier crossing and independent of medium viscosity and substituent size. This result is strikingly different to similar measurements made on first generation molecular motors, suggesting changes in the rotation mechanism between the two generations.

EXPERIMENTAL SECTION

Measurements. The ultrafast up-conversion apparatus used to measure time-resolved fluorescence with 50 fs time resolution was described in detail elsewhere.[43] For all ultrafast measurements, the excitation wavelength was 400 nm, power was 8 mW and the sample concentration was 0.5 mM. All samples were flowed continuously in a 1 mm path length cell for the duration of the measurement. Steady state fluorescence spectra were recorded at lower concentrations (tens of micromolar) and Raman and solvent contributions were subtracted in each case. For the ground state kinetics studies, time-resolved absorption measurements (Ocean Optics USB2000) were made with samples (tens of micromolar) in a 1 cm path length cell, excited by a 405 nm LED lamp with a power of 1 mW.

Design of the Molecules. The molecules intended for this investigation had to fulfill several conditions. First of all, substitution with several rigid arms capable of interaction with solvent was required. We therefore opted for a homologous series of phenyl-ethynylene oligomers. In order to promote solubility and thus allow for sufficient absorption, branched alkyl chains were installed at the end of the rigid arms. Because of the specific excitation wavelength of the excitation laser, it was essential to ensure that the absorption maximum did not significantly bathochromically shift with the increasing conjugation of the phenyl-ethynylene oligomers. Because of this, the motor was connected to the arms using a biaryl connection. The biaryl moiety adopts a twisted conformation and was expected to severely disrupt conjugation between the motor core and rigid

DOI: 10.1021/acs.jpca.7b00087
J. Phys. Chem. A 2017, 121, 2138−2150

arms (Figure 12). For details of the synthetic procedures used to synthesize **1**−**4** see Supporting Information.

■ ASSOCIATED CONTENT

Supporting Information

The Supporting Information is available free of charge on the ACS Publications website at DOI: 10.1021/acs.jpca.7b00087.

Additional experiments on solvent dependent electronic spectra, a more complete data set on time-resolved fluorescence, and synthesis and characterization data for molecules **2**−**4** (PDF)

■ AUTHOR INFORMATION

Corresponding Authors

*(S.R.M.) E-mail: s.meech@uea.ac.uk.

*(B.L.F.) E-mail: b.l.feringa@rug.nl.

ORCID

Wesley R. Browne: 0000-0001-5063-6961

Stephen R. Meech: 0000-0001-5561-2782

Notes

The authors declare no competing financial interest.

■ ACKNOWLEDGMENTS

We are grateful to EPSRC (EP/J009148 and EP/M001997 and NanoNextNL of the Government of The Netherlands and 130 partners for financial support. Thanks also to T. D. Tiemersma-Wegman for performing the HRMS measurements.

■ REFERENCES

(1) Schliwa, M.; Woehlke, G. Molecular Motors. *Nature* **2003**, *422* (6933), 759−765.

(2) Browne, W. R.; Feringa, B. L. Making Molecular Machines Work. *Nat. Nanotechnol.* **2006**, *1* (1), 25−35.

(3) Kottas, G. S.; Clarke, L. I.; Horinek, D.; Michl, J. Artificial Molecular Rotors. *Chem. Rev.* **2005**, *105* (4), 1281−1376.

(4) Kelly, T. R.; De Silva, H.; Silva, R. A. Unidirectional Rotary Motion in a Molecular System. *Nature* **1999**, *401* (6749), 150−152.

(5) Fletcher, S. P. A Reversible, Unidirectional Molecular Rotary Motor Driven by Chemical Energy. *Science (Washington, DC, U. S.)* **2005**, *310* (5745), 80−82.

(6) Ballardini, R.; Balzani, V.; Credi, A.; Gandolfi, M. T.; Venturi, M. Artificial Molecular-Level Machines: Which Energy To Make Them Work? *Acc. Chem. Res.* **2001**, *34* (6), 445−455.

(7) Brouwer, A. M.; Frochot, C.; Gatti, F. G.; Leigh, D. A.; Mottier, L.; Paolucci, F.; Roffia, S.; Wurpel, G. W. H. Photoinduction of Fast, Reversible Translational Motion in a Hydrogen-Bonded Molecular Shuttle. *Science (Washington, DC, U. S.)* **2001**, *291* (5511), 2124−2128.

(8) Badjić, J. D.; Balzani, V.; Credi, A.; Silvi, S.; Stoddart, J. F. A Molecular Elevator. *Science (Washington, DC, U. S.)* **2004**, *303* (5665), 1845−1849.

(9) Bissell, R. A.; Cordova, E.; Kaifer, A. E.; Stoddart, J. F. A Chemically and Electrochemically Switchable Molecular Shuttle. *Nature* **1994**, *369* (6476), 133−137.

(10) Pease, A. R.; Jeppesen, J. O.; Stoddart, J. F.; Luo, Y.; Collier, C. P.; Heath, J. R. Switching Devices Based on Interlocked Molecules. *Acc. Chem. Res.* **2001**, *34* (6), 433−444.

(11) Feringa, B. L.; Koumura, N.; Zijlstra, R. W. J.; van Delden, R. a; Harada, N. Light-Driven Monodirectional Molecular Rotor. *Nature* **1999**, *401* (6749), 152−155.

(12) Feringa, B. L. In Control of Motion: From Molecular Switches to Molecular Motors. *Acc. Chem. Res.* **2001**, *34* (6), 504−513.

(13) Koumura, N.; Geertsema, E. M.; van Gelder, M. B.; Meetsma, A.; Feringa, B. L. Second Generation Light-Driven Molecular Motors. Unidirectional Rotation Controlled by a Single Stereogenic Center with Near-Perfect Photoequilibria and Acceleration of the Speed of Rotation by Structural Modification. *J. Am. Chem. Soc.* **2002**, *124* (18), 5037−5051.

(14) Vicario, J.; Meetsma, A.; Feringa, B. L. Controlling the Speed of Rotation in Molecular Motors. Dramatic Acceleration of the Rotary Motion by Structural Modification. *Chem. Commun. (Cambridge, U. K.)* **2005**, No. 47, 5910−5912.

(15) Kistemaker, J. C. M.; Štacko, P.; Visser, J.; Feringa, B. L. Unidirectional Rotary Motion in Achiral Molecular Motors. *Nat. Chem.* **2015**, *7* (11), 890−896.

(16) Conyard, J.; Addison, K.; Heisler, I. a; Cnossen, A.; Browne, W. R.; Feringa, B. L.; Meech, S. R. Ultrafast Dynamics in the Power Stroke of a Molecular Rotary Motor. *Nat. Chem.* **2012**, *4* (7), 547−551.

(17) Conyard, J.; Cnossen, A.; Browne, W. R.; Feringa, B. L.; Meech, S. R. Chemically Optimizing Operational Efficiency of Molecular Rotary Motors. *J. Am. Chem. Soc.* **2014**, *136* (27), 9692−9700.

(18) Pollard, M. M.; Wesenhagen, P. V.; Pijper, D.; Feringa, B. L. On the Effect of Donor and Acceptor Substituents on the Behaviour of Light-Driven Rotary Molecular Motors. *Org. Biomol. Chem.* **2008**, *6* (9), 1605.

(19) Chen, J.; Chen, K.-Y.; Carroll, G. T.; Feringa, B. L. Facile Assembly of Light-Driven Molecular Motors onto a Solid Surface. *Chem. Commun.* **2014**, *50* (84), 12641−12644.

(20) van Delden, R. a; ter Wiel, M. K. J.; Pollard, M. M.; Vicario, J.; Koumura, N.; Feringa, B. L. Unidirectional Molecular Motor on a Gold Surface. *Nature* **2005**, *437* (7063), 1337−1340.

(21) Pollard, M. M.; ter Wiel, M. K. J.; van Delden, R. A.; Vicario, J.; Koumura, N.; van den Brom, C. R.; Meetsma, A.; Feringa, B. L. Light-Driven Rotary Molecular Motors on Gold Nanoparticles. *Chem. - Eur. J.* **2008**, *14* (36), 11610−11622.

(22) Kudernac, T.; Ruangsupapichat, N.; Parschau, M.; Maciá, B.; Katsonis, N.; Harutyunyan, S. R.; Ernst, K.-H.; Feringa, B. L. Electrically Driven Directional Motion of a Four-Wheeled Molecule on a Metal Surface. *Nature* **2011**, *479* (7372), 208−211.

(23) Zhao, D.; Neubauer, T. M.; Feringa, B. L. Dynamic Control of Chirality in Phosphine Ligands for Enantioselective Catalysis. *Nat. Commun.* **2015**, *6*, 6652.

(24) Chen, J.; Kistemaker, J. C. M.; Robertus, J.; Feringa, B. L. Molecular Stirrers in Action. *J. Am. Chem. Soc.* **2014**, *136* (42), 14924−14932.

(25) Barrientos, H.; Arias, E.; Moggio, I.; Romero, J.; Rodríguez, O.; Giorgetti, E.; Rosso, T. Del. Dodecanoxy-Phenylethynylene Oligomers for Light Emitting Diodes. *Synth. Met.* **2004**, *147* (1−3), 267−270.

(26) Yamaguchi, Y.; Ochi, T.; Miyamura, S.; Tanaka, T.; Kobayashi, S.; Wakamiya, T.; Matsubara, Y.; Yoshida, Z. Rigid Molecular Architectures That Comprise a 1,3,5-Trisubstituted Benzene Core and Three Oligoaryleneethynylene Arms: Light-Emitting Characteristics and π Conjugation between the Arms. *J. Am. Chem. Soc.* **2006**, *128* (14), 4504−4505.

(27) Nguyen, H. T.; Huong, V. T. T.; Nguyen, M. T. Silole-Based Oligomers as Electron Transport Materials. *Chem. Phys. Lett.* **2012**, *550*, 33−40.

(28) Yamaguchi, Y.; Matsubara, Y.; Ochi, T.; Wakamiya, T.; Yoshida, Z. How the π Conjugation Length Affects the Fluorescence Emission Efficiency. *J. Am. Chem. Soc.* **2008**, *130* (42), 13867−13869.

(29) Samori, S.; Tojo, S.; Fujitsuka, M.; Spitler, E. L.; Haley, M. M.; Majima, T. Donor−Acceptor-Substituted Tetrakis(phenylethynyl)-benzenes as Emissive Molecules during Pulse Radiolysis in Benzene. *J. Org. Chem.* **2007**, *72* (8), 2785−2793.

(30) Beeby, A.; Findlay, K.; Low, P. J.; Marder, T. B. A Re-Evaluation of the Photophysical Properties of 1,4-Bis(phenylethynyl)benzene: A Model for Poly(phenyleneethynylene). *J. Am. Chem. Soc.* **2002**, *124* (28), 8280−8284.

(31) Mokhtari, A.; Chebira, A.; Chesnoy, J. Subpicosecond Fluorescence Dynamics of Dye Molecules. *J. Opt. Soc. Am. B* **1990**, *7* (8), 1551.

(32) Pollard, W. T.; Lee, S.-Y.; Mathies, R. a. Wave Packet Theory of Dynamic Absorption Spectra in Femtosecond Pump−probe Experiments. *J. Chem. Phys.* **1990**, *92* (7), 4012.

(33) Rubtsov, I. V.; Yoshihara, K. Vibrational Coherence in Electron Donor - Acceptor Complexes. *J. Phys. Chem. A* **1999**, *103*, 10202−10212.
(34) Kazaryan, A.; Filatov, M. Density Functional Study of the Ground and Excited State Potential Energy Surfaces of a Light-Driven Rotary Molecular Motor. *J. Phys. Chem. A* **2009**, *113*, 11630−11634.
(35) Kazaryan, A.; Kistemaker, J. C. M.; Schäfer, L. V.; Browne, W. R.; Feringa, B. L.; Filatov, M. Understanding the Dynamics Behind the Photoisomerization of a Light-Driven Fluorene Molecular Rotary Motor. *J. Phys. Chem. A* **2010**, *114*, 5058−5067.
(36) Kazaryan, A.; Lan, Z.; Schäfer, L. V.; Thiel, W.; Filatov, M. Surface Hopping Excited-State Dynamics Study of the Photoisomerization of a Light-Driven Fluorene Molecular Rotary Motor. *J. Chem. Theory Comput.* **2011**, *7* (7), 2189−2199.
(37) Pang, X.; Cui, X.; Hu, D.; Jiang, Z.; Zhao, D.; Lan, Z.; Li, F. "Watching" the Dark State in Ultrafast Nonadiabatic Photoisomerization Process of a Light-Driven Molecular Rotary Motor. *J. Phys. Chem. A* **2017**, *121*, 1240.
(38) Doolittle, A. K. Studies in Newtonian Flow. II. the Dependence of the Viscosity of Liquids on Free-Space. *J. Appl. Phys.* **1951**, *22* (12), 1471−1475.
(39) Velsko, S. P.; Fleming, G. R. Photochemical Isomerization in Solution. Photophysics of Diphenyl Butadiene. *J. Chem. Phys.* **1982**, *76* (7), 3553.
(40) Velsko, S. P. Breakdown of Kramers Theory Description of Photochemical Isomerization and the Possible Involvement of Frequency Dependent Friction. *J. Chem. Phys.* **1983**, *78* (1), 249.
(41) Bagchi, B. The Effect of Frequency Dependent Friction on Isomerization Dynamics in Solution. *J. Chem. Phys.* **1983**, *78* (5), 2735.
(42) Bauer, J.; Hou, L.; Kistemaker, J. C. M.; Feringa, B. L. Tuning the Rotation Rate of Light-Driven Molecular Motors. *J. Org. Chem.* **2014**, *79* (10), 4446−4455.
(43) Heisler, I. A.; Kondo, M.; Meech, S. R. Reactive Dynamics in Confined Liquids: Ultrafast Torsional Dynamics of Auramine O in Nanoconfined Water in Aerosol OT Reverse Micelles. *J. Phys. Chem. B* **2009**, *113* (6), 1623−1631.

DOI: 10.1021/acs.jpca.7b00087
J. Phys. Chem. A 2017, 121, 2138−2150